Inverse Landau-Zener-Stückelberg problem for qubit-resonator systems

S. N. Shevchenko, S. Ashhab, and Franco Nori

Phys. Rev. B **85**, 094502 — Published 2 March 2012

DOI: 10.1103/PhysRevB.85.094502

Inverse Landau-Zener-Stückelberg problem for qubit-resonator systems

S. N. Shevchenko,[1,2,*] S. Ashhab,[2,3] and Franco Nori[2,3]

[1]*B.Verkin Instiute for Low Temperature Physics and Engineering, Kharkov, Ukraine*
[2]*RIKEN Advanced Science Institute, Wako-shi, Saitama, Japan*
[3]*Department of Physics, The University of Michigan, Ann Arbor, Michigan, USA*

(Dated: January 10, 2012)

We consider theoretically a superconducting qubit - nanomechanical resonator (NR) system, which was realized by LaHaye et al. [Nature **459**, 960 (2009)]. First, we study the problem where the state of the strongly driven qubit is probed through the frequency shift of the low-frequency NR. In the case where the coupling is capacitive, the measured quantity can be related to the so-called quantum capacitance. Our theoretical results agree with the experimentally observed result that, under resonant driving, the frequency shift repeatedly changes sign. We then formulate and solve the inverse Landau-Zener-Stückelberg problem, where we assume the driven qubit's state to be known (i.e. measured by some other device) and aim to find the parameters of the qubit's Hamiltonian. In particular, for our system the qubit's bias is defined by the NR's displacement. This may provide a tool for monitoring of the NR's position.

I. INTRODUCTION

Nanoelectromechanical systems have recently attracted attention because of both possible applications (e.g. in sensing) and interest in fundamental quantum phenomena in mesoscopic systems.[1] Particularly interesting is the coupling of the mechanical motion of a nanomechanical resonator (NR) to an electric mesoscopic system. A few examples are carbon nanotube NRs coupled to electron transport[2] and a metallic NR coupled to an LC tank circuit[3]. It was proposed theoretically that for sensing and controlling the NRs, superconducting few-level circuits (qubits)[4] can be effectively used.[5,6] For example this approach was applied in the demonstration of the ground state of a high-frequency piezoelectric dilatational resonator coupled to a superconducting phase qubit.[7]

Successful coupling of a NR (a suspended silicon nitride beam) to a charge qubit allowed LaHaye *et al.* [8] to demonstrate both ground-state measurement and excited-state spectroscopy as well as Landau-Zener-Stückelberg (LZS) interferometry of the qubit. The spectroscopy was performed with weak driving, where the position of the resonance gave the information about the qubit levels. In the regime of strong driving, where the qubit's evolution experiences repeated LZS transitions at the avoided crossing, the resulting interference is visualized in the LZS interferograms [9]. The LZS interferometry was demonstrated on superconducting qubits probed by different methods (see Ref. [9] and references therein), as well as studied for other different physical realizations of strongly-driven two-level systems in Refs. [10].

In the work by LaHaye *et al.*, Ref. [8], the NR's frequency shift was used for monitoring the qubit's state. For the theoretical description of the NR-qubit system, the perturbation-theory procedure developed in Ref. [5] was used. The theory says that the NR's frequency shift $\Delta\omega_{\rm NR}$ is negative for the qubit in the ground state and zero when the two qubit states are on average equally populated under the periodic driving. This allowed to describe the ground-state and low-amplitude spectroscopy measurements.[8] However, this theory does not explain the experimentally observed sign changes of $\Delta\omega_{\rm NR}$ in the strong-driving regime, where the frequency shift becomes positive.

In this work we consider the NR-qubit system semi-classically. Within this approach, we describe the qubit as a quantum system coupled to a classical resonator, with the oscillation-energy quantum much smaller than the thermal energy, $\hbar\omega_{\rm NR} \ll k_B T$. Note that such a semi-classical approach was successful for the description of most phenomena related to atom-light interaction.[11]

The impact of the qubit on the resonator's frequency shift can be described in terms of the so-called quantum capacitance, as studied for the qubits in Refs. [12,13]. The quantum capacitance is defined as the derivative of the average charge on the qubit with respect to the applied voltage. The charge can then be related to the charge-qubit occupation, the derivative of which (under resonant driving) exhibits sign changes. Similar sign-changing response under strong driving was recently studied for qubits probed by an LC (tank) circuit for capacitive coupling[14,15] as well as for inductive coupling[16,17]. Thus, in the first part of this work (Section II) we study the situation where the strong-driving qubit's state is probed by the NR.

In Section III, we formulate the inverse problem. There, we are interested in the influence of the NR's state (its position) on the qubit's state. We graphically demonstrate the formulation of the problem for the direct and inverse interferometry in Fig. 1. There, the two-level system represents a qubit with control parameter ε_0; the parabola represents the resonator's potential energy as a function of the displacement x. Thus, in the first part of our work (Sec. II) we deal with the direct problem, where the influence of the qubit's state on the resonator is studied.

The second part of this work (Secs. III and IV) is devoted to the inverse problem, where we study the influence of the resonator's state on the qubit's state. Measuring the latter is an alternative method for defining the NR's displacement. This approach can be related also to other inverse problems for two-level systems, as studied in Refs. [18–20]. Generalization of the results can also be applied to other quantum systems for which the problem of defining the Hamiltonian's parameters with given system's state was studied in Ref. [21]. In Section IV we demonstrate how the inverse problem can be solved for

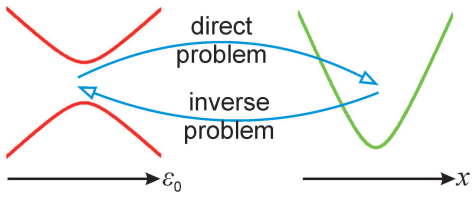

FIG. 1: (Color online) Schematic representation of the formulated problems for direct and inverse interferometry. The red curves on the left represent the bias-dependent energy levels of the qubit, and the green parabola on the right shows the potential energy of the (classical) resonator. In the direct problem, the resonator is used to probe the state of the qubit. In the inverse problem, the response of the qubit to external driving is used to infer the state of the resonator.

different driving regimes in a generic two-level system, and we comment on the possibility of applying this technique for superconducting qubit-NR systems.

II. CHARGE QUBIT PROBED THROUGH THE QUANTUM CAPACITANCE

The split-junction charge qubit (also called Cooper-pair box and shown in red in Fig. 2) consists of a small island between two Josephson junctions. The state of the qubit is controlled by the magnetic flux Φ and the gate voltage $V_{\rm CPB}+V_{\rm MW}$. Here $V_{\rm CPB}$ is the dc voltage used to tune the energy levels of the qubit and $V_{\rm MW}=V_\mu\sin\omega t$ is the microwave signal used to drive and manipulate the energy-level occupations. The Cooper-pair box is described in the two-level approximation by the Hamiltonian in the charge representation (see e.g. Ref. [8] and Appendix A)

$$H(t)=-\frac{\Delta}{2}\sigma_x-\frac{\varepsilon_0}{2}\sigma_z-\frac{A\sin\omega t}{2}\sigma_z. \qquad (1)$$

Here the tunnel splitting Δ is equal to the Josephson energy $E_{\rm J}$, which is controlled by the magnetic flux Φ

$$\Delta\equiv E_{\rm J}=E_{\rm J0}\left|\cos(\pi\Phi/\Phi_0)\right|. \qquad (2)$$

The charging energy and the driving amplitude are given by

$$\varepsilon_0=8E_{\rm C}(n_{\rm g}-1/2),\qquad A=8E_{\rm C}n_\mu, \qquad (3)$$

where the Coulomb energy $E_{\rm C}=e^2/2C_\Sigma$ is defined by the total island's capacitance $C_\Sigma=2C_{\rm J}+C_{\rm CPB}+C_{\rm NR}$, defined with the notation $2C_{\rm J}\equiv C_{\rm J1}+C_{\rm J2}$; the dimensionless driving amplitude is $n_\mu=C_{\rm CPB}V_\mu/2e$; the dimensionless polarization charge $n_{\rm g}=n_{\rm NR}+n_{\rm CPB}$ is the fractional part of the respective polarization charges in the plates of two capacitors: $n_{\rm NR}=\{N_{\rm NR}\}$ and $n_{\rm CPB}=\{N_{\rm CPB}\}$ with $N_{\rm NR}=C_{\rm NR}V_{\rm NR}/2e$ and $N_{\rm CPB}=C_{\rm CPB}V_{\rm CPB}/2e$.

Here we consider the Cooper-pair box formed by four capacitances, $C_{\rm J1}$, $C_{\rm J2}$, $C_{\rm CPB}$, and $C_{\rm NR}$ ($C_{\rm J}\gg C_{\rm CPB},C_{\rm NR}$). One of the plates of the latter capacitor is formed by the NR, which is characterized by the displacement at the midpoint

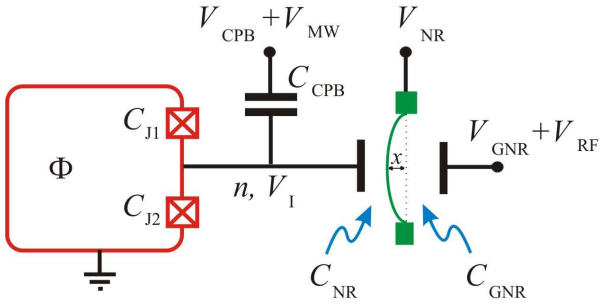

FIG. 2: (Color online) Schematic diagram of a split-junction charge qubit coupled to a nanomechanical resonator. The charge qubit (shown in red) is biased by the magnetic flux Φ and the dc+μw voltage $V_{\rm CPB}+V_{\rm MW}$, to which it is coupled through the capacitance $C_{\rm CPB}$. The qubit is coupled to the NR (shown in green) through the capacitance $C_{\rm NR}$. The NR is biased by a large dc voltage $V_{\rm NR}$; its state is controlled and measured by applying the dc and rf voltages between the gate and the NR, $V_{\rm GNR}$ and $V_{\rm RF}$, through the capacitance $C_{\rm GNR}$. The NR's motion is described by the displacement at the midpoint x. Capacitances form the island (Cooper-pair box) with the total capacitance C_Σ, voltage V_I and charge $-2en$.

x. This displacement is much smaller than the distance d between the plates, in which case the capacitance between the NR and the qubit reads

$$C_{\rm NR}(x)\approx C_{\rm NR0}+\left.\frac{\partial C_{\rm NR}}{\partial x}\right|_0 x\equiv C_{\rm NR0}\left(1+\frac{x}{\xi}\right), \qquad (4)$$

$$\xi^{-1}=\frac{1}{C_{\rm NR0}}\left.\frac{\partial C_{\rm NR}}{\partial x}\right|_0,\ \ \xi\sim d\gg x. \qquad (5)$$

(By the subscript 0 here we mean the values at $x=0$; in what follows this subscript is assumed). The displacement of the NR influences the qubit through the changes in the polarization charge; to make this influence significant, a large dc voltage $V_{\rm NR}$ (of the order of volts) is applied. On the other side, the NR is biased by dc and rf voltages, $V_{\rm GNR}$ and $V_{\rm RF}$, through the capacitance $C_{\rm GNR}$.

The influence of the qubit's dynamics on the nanomechanical resonator can be described in different ways. In Appendix A we present a detailed derivation of the influence of the qubit's state through the voltage $V_{\rm I}$ and the average polarization charge $-2e\langle n\rangle$ of the CPB on the NR's dynamics. An alternative, and maybe physically more illustrative, approach is to describe the CPB as an effective capacitor, which is the subject of Appendix B. Here, in the main text, we present only essential results, referring the interested reader to the Appendices.

As a result of the interaction between the qubit and the NR, the resonance frequency of the NR is shifted (see Appendix A). The result can be written in the following form

$$\frac{\Delta\omega_{\rm NR}}{\omega_{\rm NR}}=-\beta\frac{\partial\langle n\rangle}{\partial n_{\rm g}}=-\frac{\beta}{2}\frac{\partial\langle\sigma_z\rangle}{\partial n_{\rm g}}, \qquad (6)$$

$$\beta=\frac{1}{m\omega_{\rm NR}^2C_\Sigma}\left(\frac{C_{\rm NR}V_{\rm NR}}{\xi}\right)^2. \qquad (7)$$

The frequency shift $\Delta\omega_{\rm NR}$ is defined by the *derivative* of the average extra Cooper-pair number on the island $\langle n\rangle = 0\cdot P_0 + 1\cdot P_1 = P_1$. Here P_0 (P_1) stands for the probability of having 0 (1) extra Cooper pair.

Alternatively to the approach above, the effect of the qubit on the NR can be described in terms of the effective (differential) capacitance, as described in Appendix B, $C_{\rm eff} = \partial Q_{\rm NR}/\partial V_{\rm NR} = C_{\rm geom} + C_{\rm Q}$, where the relevant *quantum* capacitance is given by

$$C_{\rm Q} = \frac{C_{\rm NR}^2}{C_\Sigma}\frac{\partial\langle n\rangle}{\partial n_{\rm g}}. \tag{8}$$

The term "quantum" capacitance is used here to denote the (small) qubit-state-dependent addition to the classical (geometric) capacitance. Obviously, Eq. (6) can be rewritten in terms of the quantum capacitance (*cf.* discussion in Appendix C for the qubit-LCR circuit system)

$$\frac{\Delta\omega_{\rm NR}}{\omega_{\rm NR}} = -\widetilde{\beta}\frac{C_{\rm Q}}{C_{\rm NR}}, \tag{9}$$

where $\widetilde{\beta} = (C_\Sigma/C_{\rm NR})\,\beta$.

The qubit's density matrix in the energy representation (in the eigenbasis of the time-independent Hamiltonian) is parameterized in terms of the respective Pauli matrices τ_i as follows: $\rho = \frac{1}{2}\left(X\tau_x + Y\tau_y + Z\tau_z\right)$. Now we express the probability of having one excess Cooper pair, P_1, by changing from the energy basis to the charge basis, and obtain

$$P_1 = \frac{1}{2}\left(1 - \frac{\Delta}{\Delta E}X + \frac{\varepsilon_0}{\Delta E}Z\right),\ \Delta E = \sqrt{\Delta^2+\varepsilon_0^2}. \tag{10}$$

And this gives (after time-averaging over the driving period $2\pi/\omega$) for the quantum capacitance the following

$$C_{\rm Q} \approx \frac{C_{\rm NR}^2}{C_\Sigma}\left(\frac{4E_{\rm C}\Delta^2}{\Delta E^3}Z + \frac{\varepsilon_0}{2\Delta E}\frac{\partial Z}{\partial n_{\rm g}}\right), \tag{11}$$

where we have taken into account that in the stationary state X averages to 0.[9]

As we can see from Eq. (11), the quantum capacitance is defined by the value $Z = \langle\tau_z\rangle$ which is the difference between the occupation probabilities of the excited and ground states. In particular, we obtain the quantum capacitance and the respective frequency shift in the ground/excited (g/e) state with $Z = \langle\tau_z\rangle = \pm 1$

$$\frac{\Delta\omega_{\rm NR}^{\rm g/e}}{\omega_{\rm NR}} = \mp\beta\frac{4E_{\rm C}\Delta^2}{\Delta E^3}. \tag{12}$$

This result, obtained in the semi-classical approach, is in agreement with the one obtained in Ref. 5 and used in Ref. 8. Equation (11) is a more general result, where the second term describes the sign-changing behavior near resonance. Namely, when sweeping the gate voltage $n_{\rm g}$, the quantity Z changes from -1, far from resonance (in the ground state), to 0 in resonance (when the levels are equally populated). This describes the maximum of Z in resonance and the change of its derivative $\partial Z/\partial n_{\rm g}$ from positive, in the left vicinity of the resonance, to negative, to the right of the resonance point. Thus, the resulting behavior of the observable (either $\Delta\omega_{\rm NR}$ or $C_{\rm Q}$) is defined by the competition of the two terms in Eq. (11). In what follows we will use Eq. (11) for the superposition states (which appear under driving).[14] Note that a similar approach for calculating the effective (quantum) inductance was used in Refs. 16,17.

The dissipative dynamics can be described with the Bloch equations written in the energy representation (where relaxation appears naturally). To characterize dissipation we use a result of the spin-boson model with the spectral density defined with the dimensionless parameter α, $J(\omega) = \alpha\hbar\omega$, (see e.g. Ref. 23 and references therein) and also introduce the (relatively large) phenomenological parameter B to describe the low-frequency $1/f$ noise:

$$T_1^{-1} = \alpha\frac{\Delta^2}{2\hbar\Delta E}\coth\frac{\Delta E}{2k_BT}, \tag{13}$$

$$T_2^{-1} = \frac{1}{2}T_1^{-1} + \frac{k_BT}{\hbar}\frac{\varepsilon_0^2}{\Delta E^2}(\alpha + \frac{B}{2\pi}) \approx B\frac{k_BT}{h}\frac{\varepsilon_0^2}{\Delta E^2}. \tag{14}$$

We display the direct LZS interferometry in Fig. 3, where the resonator's frequency shift $\Delta\omega_{\rm NR}$ was calculated with Eqs. (9) and (11). Figure 3 demonstrates that our formalism is valid for a description of the experimentally measurable quantities: the quantum capacitance or the resonant frequency shift[8,14] (see also Appendix C). Such a description allows to correctly find the position of the resonance peaks in the interferogram and to demonstrate the sign-changing behavior of the quantum capacitance, which relates to the measurable quantities. The appearance of the interferogram depends on several factors: the values of the qubit parameters, the model for the dissipative environment (such as Eqs. (13, 14) and the parameters α and B), the value of the bias current (which distorts the shape of the resonances, as demonstrated in Ref. [17]). Moreover, the formalism presented above is valid for the case where the qubit's dynamics is much faster than the NR's dynamics; otherwise one should study the cooperative dynamics of the composite system; see, e.g., discussions in Refs. [14] and [17]. However, we will not go here into more detailed calculations, since our aim was to demonstrate the simplest approach for the description of the experiment in Ref. [8].

III. THE BIAS INFLUENCED BY THE RESONATOR: PROBLEM FOR THE INVERSE INTERFEROMETRY

Let us now consider the qubit's bias ε_0, Eq. (3), as a function of the NR's displacement x. For small $x \ll \xi$, we have the expansion (4), which results in the decomposition of the bias

$$\varepsilon_0(x) \approx \varepsilon_0^*(n_{\rm g}) + \delta\varepsilon_0(x), \tag{15}$$

where

$$\varepsilon_0^*(n_{\rm g}) = 8E_{\rm C}\left(n_{\rm g} - 1/2\right), \tag{16}$$

$$\delta\varepsilon_0(x) = 8E_{\rm C}\,n_{\rm NR}\frac{x}{\xi}. \tag{17}$$

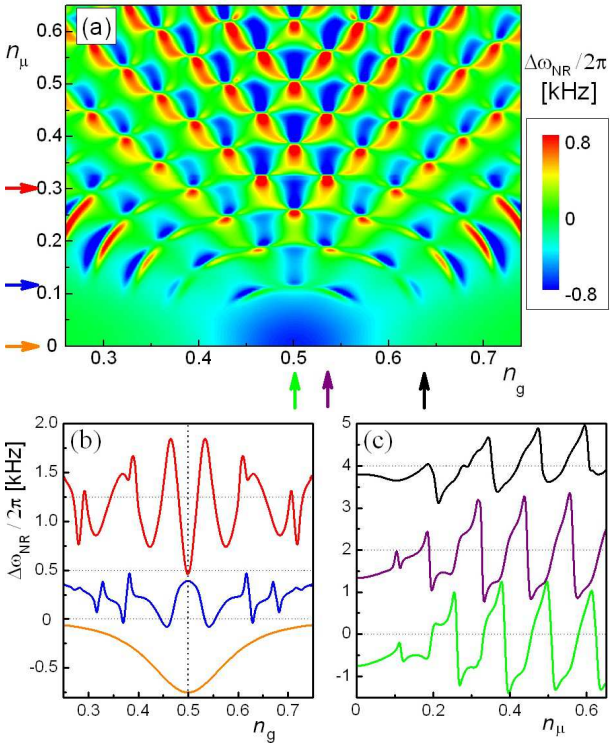

FIG. 3: (Color online) LZS interferometry probed via the resonator's frequency shift $\Delta\omega_{\rm NR}$. (a) The frequency shift versus the energy bias ($n_{\rm g}$) and the driving amplitude (n_μ). Arrows show the values of n_μ and $n_{\rm g}$ at which the graphs (b) and (c) are plotted as functions of $n_{\rm g}$ and n_μ, respectively. The upper curves were shifted for clarity. The parameters for calculations were taken close to the ones of Ref. [8]: $\omega_{\rm NR}/2\pi = 58$ MHz, $E_{\rm J0}/h = 13$ GHz, $E_{\rm C}/h = 14$ GHz, $\omega/2\pi = 4$ GHz, $k_BT/h = 2$ GHz, $\alpha = 0.005$, $B = 0.2$, and the proportionality coefficient β defined by the qubit-NR coupling constant λ from Ref. [8]: $\hbar\lambda^2/\pi E_{\rm J0} = \beta \cdot E_{\rm C}\omega_{\rm NR}/\pi E_{\rm J0} = 1.6$ kHz.

Here we have used the fact that $x \ll \xi$ and $C_{\rm NR} \ll C_\Sigma$.

The Hamiltonian of the qubit (1) with the parameter-dependent bias $\varepsilon_0(x)$ brings us to the following problem. Let us assume that the qubit's state is known (i.e., this is measured by a device whose details we do not consider here for simplicity; see Refs. [12,13,16,24] for different realizations of the ways to probe the qubit's state). Given the known qubit state, we aim to find the Hamiltonian's parameters. Particularly, we are interested in the parameter-dependent bias $\varepsilon_0(x)$.

On one hand, we can study here the general ("reverse engineering") problem in the spirit of Refs. [18,19]. On the other hand, we aim to provide the basis for measuring the NR's position x by means of probing the qubit's state, while $x = x(t)$ is considered a slow time-dependent function.

In what follows we will consider the driven qubit's state with emphasis on finding optimal driving and controlled offset parameters (A, ω, and ε_0^*) for the resolution of the small bias component $\delta\varepsilon_0$. We will assume that the dynamics of the parameter x is slow enough not to be considered during the measurement process. Depending on this slowness, the measurement might have to involve only one passage of the avoided crossing, or it can involve long-time driving and stationary-state equilibrium of the qubit. Our aim is to find a sensitive probe for small $\delta\varepsilon_0$. For high sensitivity we require substantial changes in the qubit's state for small changes of ε_0 given by $\delta\varepsilon_0$. For a quantitative definition of the sensitivity one can consider the derivative of the probability with respect to the bias ε_0.

IV. RESULTS FOR THE INVERSE LZS INTERFEROMETRY

In this section we consider the inverse problem for the qubit's dynamics, in particular how to infer the qubit's bias ε_0 from the measured qubit state. For concreteness, we consider the qubit driven by the bias $\varepsilon(t) = \varepsilon_0 + A\sin\omega t$. If one is interested in the short time-scale dynamics, then the one- or few-times passage of the avoided level crossing is relevant. If the time-dependence of the bias $\varepsilon_0(x)$ is so slow that the multiple-passage dynamics is relevant, then the stationary qubit state can be considered.

A. Single passage: non-linearity in the Landau-Zener problem

The linearization of the bias in the vicinity of the avoided crossing (where $\varepsilon(t) = 0$) results in the approximation that this region is swept at the ε_0-dependent rate $A\omega\sqrt{1-(\varepsilon_0/A)^2}$ (for details see Ref. [9]). The respective probability of the non-adiabatic transition to the upper adiabatic level is given by the Landau-Zener formula

$$P_+^{(I)} = P_{\rm LZ} = \exp\left(-\frac{\gamma}{\sqrt{1-(\varepsilon_0/A)^2}}\right),\ \gamma = \frac{\pi}{2}\frac{\Delta^2}{A\hbar\omega}. \tag{18}$$

In other words, the non-linear dependence of the bias on time has the effect that the Landau-Zener probability depends on ε_0 (see also Ref. [25]), which is demonstrated in Fig. 4(a). We note that here $|\varepsilon_0| < A$ and the formula (18) gives numerically incorrect results when ε_0 tends to A.

To quantify the sensitivity of the transition probability to small changes in the bias, in Fig. 4(c) we plot the derivative of the excitation probability $P_+^{(I)}$ with respect to ε_0. We can see that the non-linearity of the bias results in an increase of the sensitivity.

For the single-passage case it is straightforward, from Eq. (18), to find the solution for the inverse problem $\varepsilon_0 = \varepsilon_0(P_+^{(I)})$. In particular, in the case $\varepsilon_0^* = 0$ and $\delta\varepsilon_0 \ll A$ we have

$$P_{\rm LZ} \approx P_{\rm LZ,0}\left[1 - \frac{\gamma}{2}\left(\frac{\delta\varepsilon_0}{A}\right)^2\right],\ P_{\rm LZ,0} = e^{-\gamma}, \tag{19}$$

and the solution for the inverse problem becomes

$$\frac{\delta\varepsilon_0}{A} = \sqrt{\frac{2}{\gamma}\left(1 - \frac{P_{\rm LZ}}{P_{\rm LZ,0}}\right)}. \tag{20}$$

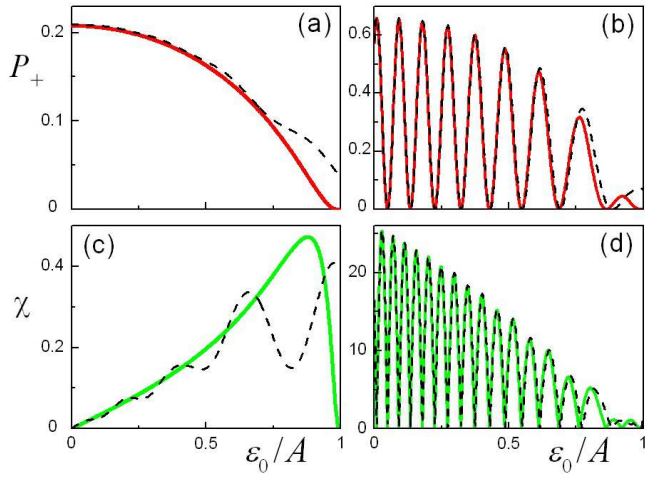

FIG. 4: (Color online) Upper-level excitation probability P_+ after (a) single passage and (b) double passage, plotted for $A/\Delta = 5$ and $\hbar\omega/\Delta = 0.2$, versus the bias ε_0. The sensitivity to the changes of the bias ε_0, defined as the derivative, $\chi = |dP_+/d(\varepsilon_0/A)|$, is plotted in (c) and (d), respectively. Solid lines were plotted with Eqs. (18) and (21), while dashed lines were calculated numerically.

B. Double passage: Stückelberg oscillations

Next, consider the situation where the avoided crossing region is passed twice. For example, the qubit can be driven by a sinusoidal pulse of length $2\pi/\omega$. Alternatively, triangular pulses can be used to drive the qubit twice through the avoided-level crossing, as in Refs. [26,27]. In both cases, the double-passage process can make use of quantum interference to increase the sensitivity of our problem through the accumulation of the Stückelberg phase.[28]

The upper-level excitation probability after the double-passage is[9]

$$P_+^{(II)} = 4P_{\rm LZ}(1-P_{\rm LZ})\sin^2(\zeta_2+\varphi_{\rm S}), \qquad (21)$$

where ζ_2 is the phase acquired during the evolution between anticrossings at t_2 and $t_1 + 2\pi/\omega$:

$$\zeta_2 = \frac{1}{2\hbar}\int_{t_2}^{t_1+2\pi/\omega}\sqrt{\Delta^2+\varepsilon(t)^2}\,dt, \qquad (22)$$

and $\varphi_{\rm S}$ is the Stokes phase.

Stückelberg oscillations, described by Eq. (21), are demonstrated in Fig. 4(b) for $0 < \varepsilon_0/A < 1$. The respective sensitivity is shown in Fig. 4(d). The agreement of the analytical formulas and numerical calculations is remarkable (as demonstrated in Fig. 4). One can notice that the sharper the Stückelberg oscillations, the higher the sensitivity. This is related to the period of the Stückelberg oscillations, which decreases with increasing A/ω. Here we also note that $P_+^{(II)}(\varepsilon_0)$ is not a symmetric function, and the period of the Stückelberg oscillations is smaller for $\varepsilon_0 < 0$ than for $\varepsilon_0 > 0$. Therefore, using negative values of ε_0 results in slightly higher sensitivity than what is shown in Fig. 4(d).

The factor $P_{\rm LZ}(1-P_{\rm LZ})$ in Eq. (21) is described by the one-passage problem above. Consider the term $\cos^2\zeta_2$. For $\varepsilon_0^* = 0$ and $\delta\varepsilon_0 \ll A$ we have[9] $\zeta_2 \approx \frac{A}{\hbar\omega} - \frac{\pi}{2}\frac{\delta\varepsilon_0}{\hbar\omega}$. For example, for $\frac{A}{\hbar\omega} = 2k\pi + \frac{\pi}{4}$ we obtain

$$P_+^{(II)} \approx 2P_{\rm LZ}(1-P_{\rm LZ})\left(1+\pi\frac{\delta\varepsilon_0}{\hbar\omega}\right). \qquad (23)$$

This describes a linear dependence on the small bias $\delta\varepsilon_0$, which is a significant increase in sensitivity as compared to the quadratic dependence on $\delta\varepsilon_0$ in the single-passage case above, Eq. (19). If the decoherence is negligibly small, one can further increase the sensitivity of the excitation probability to small changes in the bias due to interference by considering multiple-passage case.

The formula (23) can be conveniently used to make quantitative estimates. Consider this for the example of the qubit-nanomechanical resonator system as in Ref. [8]. First, to increase the sensitivity of the changes of $P_+^{(II)}$ with respect to $\delta\varepsilon_0$, we choose the smallest possible frequency ω. In our case the driving period should exceed the decoherence time T_2 and the NR oscillation period $2\pi/\omega_{\rm NR}$. For superconducting qubits T_2 is typically higher than 1 μs. Then, we are limited by the relation $\omega > \omega_{\rm NR}$, and we take $\omega/2\pi \sim 0.1$ GHz. We choose the parameters $A(n_\mu)$ and $\Delta(\Phi)$ such that $P_{\rm LZ} \sim 1/2$. Assuming $n_{NR} = 1$ and $8E_C/h = 100$ GHz, we obtain the change of the probability with changes in the NR's displacement $\Delta P_+^{(II)} = 10^3 x/\xi$. This means that for probing a displacement of $x \sim 10^{-5}\xi$, one has to be able to measure population changes $P_+^{(II)} \sim 0.01$. This level of accuracy is achievable with superconducting qubits.[29]

C. Multiple passage: stationary solution

Now we assume that what is relevant for our inverse problem is the stationary state of the driven qubit. To analyze the analytical expressions, we consider two limiting cases.

1. *Slow-passage limit*

For the analytical description of the upper-level occupation probability in the adiabatic limit, when $\gamma > 1$, we use the following formula from Ref. [9]

$$\overline{P_+} = \frac{P_{\rm LZ}(1-\cos\zeta'_+\cos\zeta_-)}{\sin^2\zeta'_+ + 2P_{\rm LZ}(1-\cos\zeta'_+\cos\zeta_-)}, \qquad (24)$$

where

$$\zeta'_+ = \zeta_1+\zeta_2,\ \zeta_- = \zeta_1-\zeta_2,$$
$$\zeta_1 = \frac{1}{2\hbar}\int_{t_1}^{t_2}\sqrt{\Delta^2+\varepsilon(t)^2}dt, \qquad (25)$$

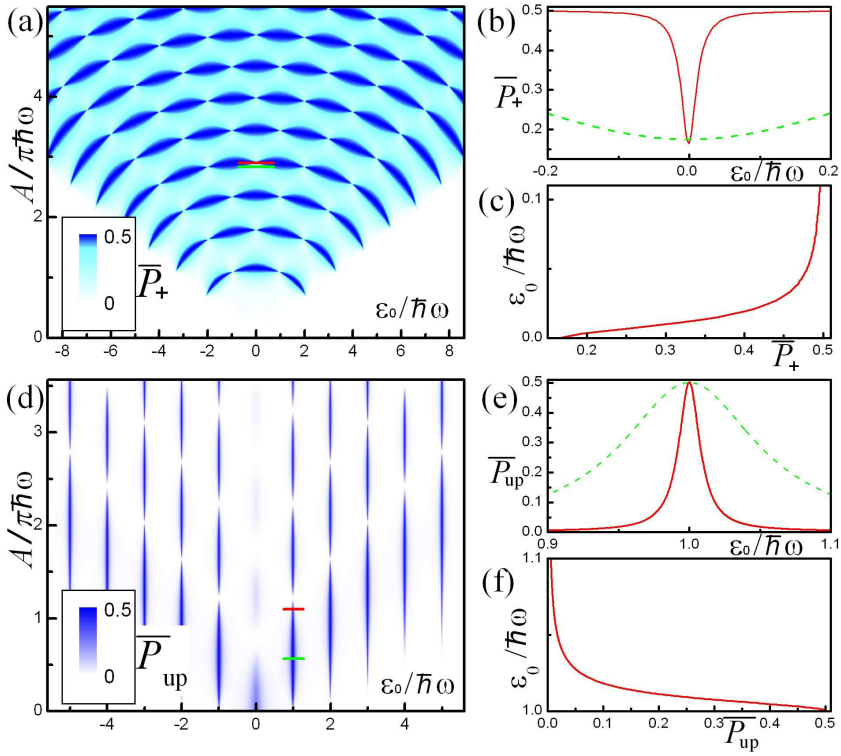

FIG. 5: (Color online) Slow-passage and fast-passage LZS interferometry of a qubit. (a) and (d): the time-averaged upper-level occupation probabilities, defined in the adiabatic ($\overline{P_+}$) and diabatic ($\overline{P}_{\rm up}$) bases, as functions of the bias ε_0 and driving amplitude A. The parameters are the same as for Fig. 3 except for the frequency: (a) $\omega/2\pi = 6.5$ GHz $< \Delta/h$ and (d) $\omega/2\pi = 20$ GHz $> \Delta/h$. (b) and (e): Cross-sections for the respective dependencies of the upper-level occupation probabilities as functions of the bias along the horizontal dashes shown in red and green in (a) and (d). (c) and (f): Inverse graphs, which show the dependence of the bias on the upper-level occupation probabilities (assuming that ε_0 lies on the right-hand side of the resonance peak).

and ζ_2 is given by Eq. (22). Formula (24) is illustrated in Fig. 5(a). Consider $\varepsilon_0^* = 0$, then for strong driving, $A \gg \Delta$, we have

$$\zeta_- \approx \frac{\pi\delta\varepsilon_0}{\hbar\omega}, \quad \zeta'_+ \approx \frac{2A}{\hbar\omega} - \frac{\delta\varepsilon_0^2}{A\hbar\omega}. \tag{26}$$

Analyzing the interferogram in Fig. 5(a), we find the possibility to obtain a sensitive working point with a driving amplitude a little bit lower than the one where the width of the resonance line tends to zero, that is $2A/\hbar\omega = 2\pi n - a$, $a \ll 1$ [see the red and green dashes in Fig. 5(a)]. It follows that

$$\overline{P_+} \approx \frac{1}{2}\frac{P_{\rm LZ}\left(\pi\delta\varepsilon_0/\hbar\omega\right)^2}{a^2 + P_{\rm LZ}\left(\pi\delta\varepsilon_0/\hbar\omega\right)^2}, \tag{27}$$

which is equal to zero at $\delta\varepsilon_0 = 0$ and quickly tends to $1/2$ with increasing $\delta\varepsilon_0$. This is demonstrated in Fig. 5(b).

2. *Fast-passage limit*

In the fast-passage and strong-driving regime (where $\gamma \ll 1$), the rotating-wave approximation gives for the upper-level occupation probability[24,30]

$$\overline{P}_{\rm up} = \frac{1}{2}\sum_k \frac{\Delta_k^2}{\frac{\hbar^2}{T_1T_2} + \frac{T_2}{T_1}(\varepsilon_0 - k\hbar\omega)^2 + \Delta_k^2}, \tag{28}$$

$$\Delta_k = \Delta J_k\left(A/\hbar\omega\right), \tag{29}$$

where J_k is the Bessel function. Formula (28) is demonstrated in Fig. 5(d). If the relaxation is not taken into account, then in the vicinity of the k-th resonance (where $\varepsilon_0^* = k\hbar\omega$) we obtain the Lorentzian dependence on the small bias shift $\delta\varepsilon_0$:

$$\overline{P}_{\rm up} = \frac{1}{2}\frac{\Delta_k^2}{\delta\varepsilon_0^2 + \Delta_k^2}. \tag{30}$$

This describes the resonance peak, $\overline{P}_{\rm up} = 1/2$, at $\delta\varepsilon_0 = 0$, which is demonstrated graphically in Fig. 5(e). Its width is defined by Δ_k and is minimized for the values of $A/\hbar\omega$ in the vicinity of the zeros of the Bessel function. With relaxation taken into account, the sensitivity is defined by the half-width

of the resonances, given by

$$\Delta\varepsilon_0^{(k)} = \frac{\sqrt{T_1 T_2 \Delta_k^2 + \hbar^2}}{T_2}. \quad (31)$$

This means that to increase the sensitivity, which is related to the sharpness of the resonances, one has to decrease the decoherence rate.

Here we note that it was assumed that the measurement time is much smaller than the resonator's period, $T_{\rm meas} \ll 2\pi/\omega_{\rm NR}$. On the other hand, to reach a stationary state, the measurement time should be larger than the relaxation time, $T_{1,2} < T_{\rm meas}$. This means that the results presented in this subsection are relevant for qubits with short relaxation times and for resonators with small frequencies. Alternatively, one should solve the problem which explicitly takes into account $x = x(t)$.

Formula (31) allows us to make estimates, as we did at the end of the previous subsection. For $A/\hbar\omega$ equal to one of the Bessel-function zeros and for $T_2 = 4{\rm ns} \ll 2\pi/\omega_{\rm NR}$, we obtain that the probability $\overline{P}_{\rm up}$ changes by about $1/4$ when the bias changes by $\Delta\varepsilon_0/h \sim 0.25$ GHz. On the other hand, we have seen that $\delta\varepsilon_0/h \sim 100(x/\xi)$ GHz. This means that in order to observe changes $x \sim 10^{-5}\xi$, one has to distinguish changes in $\overline{P}_{\rm up} \sim 10^{-3}$, which is also possible, in principle.[29]

D. Inverse interferometry: qubit probes resonator

The idea of the measurement procedure, presented in Fig. 5, could be as follows. Driving the qubit in a wide range of parameters is done first to plot the interferogram as in Fig. 5(a) and/or (d). Then a region of high sensitivity, where small changes in the qubit bias result in large changes in the final state, is chosen. Examples of such high-sensitivity regions are shown in Fig. 5(b) and/or (e).

From Fig. 5 we can see that both the slow-passage limit, demonstrated in Fig. 5(a-c), and the fast passage limit [Fig. 5(d-f)] can be used for the solution of the inverse problem. The choice of the optimal working point and its vicinity will depend on the specific parameters of the problem. For illustration, in Fig. 5(a) and (d) we marked by red and green small dashes two possibilities of having the dip in Fig. 5(b) or the peak in Fig. 5(e) being narrow (red curves) or relatively wide (green curves).

In principle, a low-amplitude slice near the bottom of Fig. 5(d) can be used to obtain a sharp resonance peak, as in Fig. 5(e). However, based on the results of Refs. [9,31], it seems that the width of the resonances might be increased more for low-amplitude driving due to the influence of the noise and decoherence. From the experimental point of view the best strategy is probably to obtain a wide range interferogram and then choose a narrow resonance.

One can now bias the qubit at a high-sensitivity point, apply a "measurement pulse" to the qubit, measure its state at the end of the pulse and extract the resonator's position x from the measured qubit's state, see Fig. 5(c) and (f), where ε_0 (which parametrically depends on x) is plotted as a function of the qubit's occupation probability.

It should be noted here that the measurement pulse, which is essentially a driving signal applied to the qubit, can take a short duration at the beginning of the measurement process. Afterwards the final state of the qubit is read out in the absence of any driving fields. As a result, issues that only affect the qubit on relatively large timescales, e.g. dephasing and the slow measurement of the qubit's state, do not affect the qubit's ability to accurately measure the instantaneous position of the resonator. It should also be noted that this measurement procedure is a single-shot type of measurement and not a continuous measurement. One could in principle use multiple qubits in order to perform multiple measurements on the state of the resonator.

V. CONCLUSIONS

We have analyzed a measurement scheme where a qubit is probed via a quantum capacitance. We demonstrated the sign-changing behavior of the quantum capacitance where the strongly-driven qubit exhibits a LZS interferogram. Our semi-classical calculations were used to describe recent experimental results[8] for the LZS interferometry of the qubit probed by a NR.

Then, motivated by the experimental work by LaHaye et al. [8], we formulated the inverse problem. The inverse LZS problem in our approach was formulated for the driven qubit as finding its bias ε_0 assuming its state to be known. More specifically, we have split the quasi-constant bias ε_0 into an externally-controlled part $\varepsilon_0^*(n_{\rm g})$ and a small part $\delta\varepsilon_0(x)$ that is to be measured. For the qubit-NR system the former can be changed through the gate voltage to realize the most efficient measurement working point; the latter was assumed to be a function of the NR's displacement x.

We have shown how the inverse problem can be used for defining the NR's displacement. First, one should find (measure) the direct LZS interferogram (in a wide range of parameters). This allows finding the qubit's parameters and choosing the optimal bias ε_0^*. Then, fixing the qubit's parameters at the optimal working point, small changes due to the slow NR's motion may be used for measuring its displacement.

Acknowledgments

SNS thanks V.I. Shnyrkov, O.G. Turutanov, and A.M. Zagoskin for useful discussions. SNS was partly supported by the NAS of Ukraine (Project No. 04/10-N) and DKNII (Project No. M/411-2011). SA and FN were partially supported by the Laboratory for Physical Science, National Security Agency, Army Research Office, NSF grant No. 0726909, JSPS-RFBR contract No. 09-02-92114, Grant-in-Aid for Scientific Research (S), MEXT Kakenhi on Quantum Cybernetics, and the JSPS-FIRST program.

Appendix A: Semi-classical theory for the qubit-resonator system

In this Appendix we consider the semi-classical theory for the qubit-NR system. The equation for the displacement x of the classical NR with effective mass m, quality factor Q, eigenfrequency ω_0 and driven by the external force F, is

$$m\frac{d^2x}{dt^2}+\frac{m\omega_0}{Q}\frac{dx}{dt}+m\omega_0^2 x=F. \tag{A1}$$

In our problem, presented in Fig. 2, the NR is influenced by the voltage difference from both sides. On one side (to the right of the NR in Fig. 2) the voltage difference contains the large constant part, $\Delta V = V_{\rm NR}-V_{\rm GNR}$, and the small rf driving component, $V_{\rm RF}=V_{\rm A}\cos\omega_{\rm rf}t$. The force due to these voltages is

$$\begin{aligned} F_{\rm GNR} &= \frac{1}{2}\frac{\partial}{\partial x}\left[C_{\rm GNR}(V_{\rm NR}-V_{\rm GNR}-V_{\rm RF})^2\right] \\ &\approx \frac{1}{2}\left(\frac{\partial C_{\rm GNR}}{\partial x}\right)\Delta V^2 - F_{\rm A}\cos\omega_{\rm rf}t, \end{aligned} \tag{A2}$$

where $F_{\rm A}=(\partial C_{\rm GNR}/\partial x)\cdot\Delta V\cdot V_{\rm A}$. From the other side (left side of the NR in Fig. 2) the voltage difference is defined by the island's voltage $V_{\rm I}$. The respective force is

$$\begin{aligned} F_{\rm NR} &= \frac{1}{2}\frac{\partial}{\partial x}\left[C_{\rm NR}(V_{\rm NR}-V_{\rm I})^2\right] \\ &\approx \frac{1}{2}\left(\frac{\partial C_{\rm NR}}{\partial x}\right)V_{\rm NR}^2 - V_{\rm NR}\frac{\partial}{\partial x}\left(C_{\rm NR}V_{\rm I}\right). \end{aligned} \tag{A3}$$

In the Coulomb-blockade regime, the voltage $V_{\rm I}$ is defined by the quantum-mechanically averaged island's charge $-2en$, which is given by the sum of the charges on the plates of the capacitors that define the island,

$$-2en = Q_{\rm J1}+Q_{\rm J2}-Q_{\rm CPB}-Q_{\rm NR}. \tag{A4}$$

For the island's voltage it follows that

$$V_{\rm I}=\frac{2e(N_{\rm g}+n_\mu\sin\omega t-n)}{C_\Sigma}, \tag{A5}$$

$$N_{\rm g}=\frac{C_{\rm NR}V_{\rm NR}}{2e}+\frac{C_{\rm CPB}V_{\rm CPB}}{2e}\equiv N_{\rm NR}+N_{\rm CPB}. \tag{A6}$$

Here we note that to obtain the charging Hamiltonian of the CPB in the two-state approximation, we consider $N_{\rm g}=N+n_{\rm g}$ close to a half-integer number, where N is the integer part of $N_{\rm g}$, and $n_{\rm g}=\{N_{\rm g}\}$ is the fractional part. Then, with $n=N+\widehat{n}$ and $n_\mu<1$, we obtain for $H_{\rm CPB}=C_\Sigma V_{\rm I}^2/2$ the charging part of Hamiltonian, Eq. (1). Here the operator for the extra Cooper-pair number $\widehat{n}=(1+\sigma_z)/2$ acts on the "charge" basis states as follows: $\widehat{n}\,|0\rangle=0$ and $\widehat{n}\,|1\rangle=|1\rangle$.

At this point we assume that the qubit's dynamics is much faster than that of the classical NR, so the equation for the NR can be averaged over the period $2\pi/\omega$ and then the NR's dynamics is defined by the time-averaged voltage

$$\overline{V}_{\rm I}=\frac{2e(n_{\rm g}-\overline{\langle n\rangle})}{C_\Sigma}. \tag{A7}$$

In what follows this time averaging is assumed.

Denoting the sum of the constant terms in Eqs. (A2, A3) as F_0, we obtain

$$F=F_0+\frac{\partial F}{\partial x}x-F_{\rm A}\cos\omega_{\rm rf}t, \tag{A8}$$

$$\frac{\partial F}{\partial x}=-\frac{2}{C_\Sigma}\left(\frac{C_{\rm NR}V_{\rm NR}}{\xi}\right)^2\left[1-\frac{\partial\langle n\rangle}{\partial n_{\rm g}}\right]. \tag{A9}$$

The term F_0 results in an (irrelevant) constant displacement of the NR, while the linear term results in the resonance frequency shift in Eq. (A1) as follows

$$m\omega_0^2-\frac{\partial F}{\partial x}\equiv m\widetilde{\omega}_{\rm NR}^2. \tag{A10}$$

Then we obtain the NR's frequency shift

$$\Delta\widetilde{\omega}_{\rm NR}=\widetilde{\omega}_{\rm NR}-\omega_0\approx\frac{1}{2m\omega_0}\frac{\partial F}{\partial x}\equiv\Delta\omega_1+\Delta\omega_2, \tag{A11}$$

where $\Delta\omega_1$ and $\Delta\omega_2$ correspond to the two terms in Eq. (A9). The term $\Delta\omega_1$ does not depend on the state of the qubit; we therefore define the qubit-state-dependent frequency shift

$$\Delta\omega_{\rm NR}=\Delta\widetilde{\omega}_{\rm NR}-\Delta\omega_1=\Delta\omega_2 \tag{A12}$$

which leads to Eq. (6).

Appendix B: Quantum capacitance

In addition to the theory presented in the previous Appendix, it is useful to consider the system qubit-resonator by introducing the quantum capacitance, which is the subject of this Appendix.

Let us introduce the effective (differential) capacitance, as it is shown in Fig. 6(a), by differentiating the charge $Q_{\rm NR}$ of the capacitance $C_{\rm NR}$ as follows[22]: $C_{\rm eff}=\partial Q_{\rm NR}/\partial V_{\rm NR}$. Then, for the charge $Q_{\rm NR}=(V_{\rm NR}-\overline{V}_{\rm I})C_{\rm NR}$ with the island's voltage given by Eq. (A7), we obtain

$$C_{\rm eff}=C_{\rm geom}+C_{\rm Q}, \tag{B1}$$

which consists of the quantum capacitance $C_{\rm Q}$, given by Eq. (8), and the geometric capacitance $C_{\rm geom}$

$$C_{\rm geom}=\frac{C_{\rm NR}(C_\Sigma-C_{\rm NR})}{C_\Sigma}\approx\frac{2C_{\rm J}C_{\rm NR}}{2C_{\rm J}+C_{\rm NR}}, \tag{B2}$$

where the latter approximation is valid for $C_{\rm CPB}\ll C_{\rm J},C_{\rm NR}$.

Alternatively to the approach of the previous Appendix, one can consider the force $F_{\rm NR}$ as the electrostatic force from the effective capacitance [see Fig. 6(b)]: $F_{\rm NR}=\frac{1}{2}\frac{\partial}{\partial x}\left(C_{\rm eff}V_{\rm NR}^2\right)$. Then the term with the quantum capacitance, in which $C_{\rm NR}^2\approx C_{\rm NR0}^2\left(1+x/\xi\right)^2$, results in the same frequency shift as obtained in the previous Appendix, Eq. (A12).

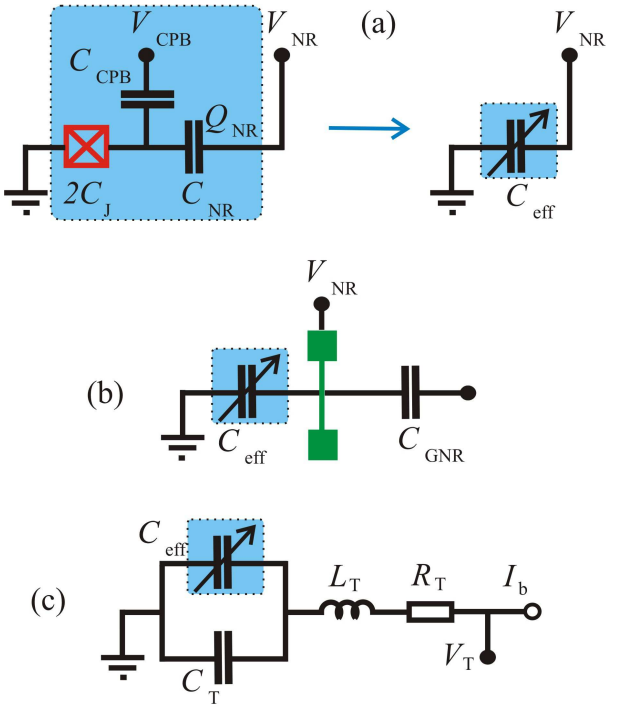

FIG. 6: (Color online) Scheme showing how the charge qubit can be described as an effective capacitance coupled either to the NR or to LCR resonator. (a) To the left, the charge qubit (CPB) is shown to be described as the capacitance $2C_{\rm J}$ controlled by the voltage $V_{\rm CPB}$ and coupled through the coupling capacitance $C_{\rm NR}$ to a measuring circuitry. This is described as the effective capacitance $C_{\rm eff}$ as shown to the right. (b) The effective capacitance is coupled to the NR, which can be used to model our system shown in Fig. 2. (c) The effective capacitance is coupled to the electric LCR tank circuit.

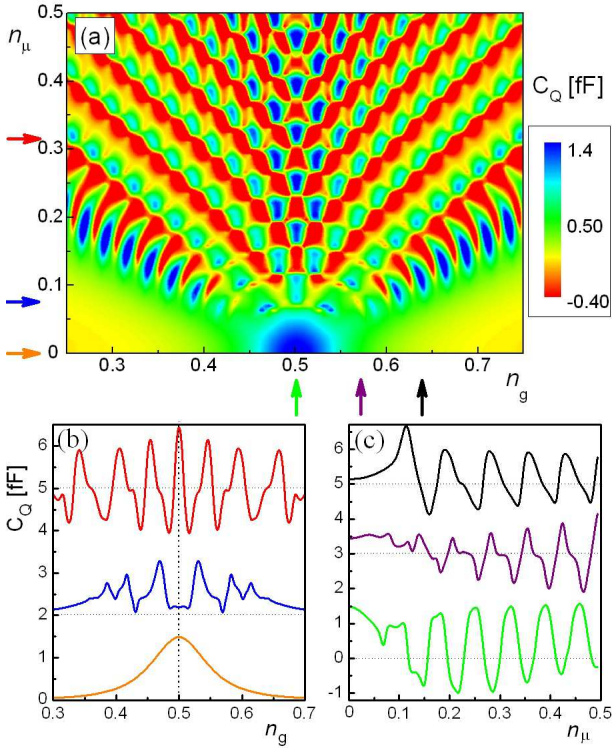

FIG. 7: (Color online) LZS interferometry probed via a quantum capacitance. (a) The quantum capacitance C_Q of the qubit versus the energy bias ($n_{\rm g}$) and the driving amplitude (n_μ). Arrows show the values of n_μ and $n_{\rm g}$ at which the graphs (b) and (c) are plotted as functions of $n_{\rm g}$ and n_μ, respectively. The upper curves were shifted for clarity.

Appendix C: Qubit probed by tank circuit

In this Appendix we consider a qubit coupled capacitively to the series LCR (tank) circuit [see Fig. 6(c)]. The tank circuit consists of an inductor $L_{\rm T}$ and a capacitor $C_{\rm T}$, while dissipation is described by the resistor $R_{\rm T}$. The qubit is considered to be coupled to the tank circuit through the coupling capacitance, which for uniformity we again denote by $C_{\rm NR}$ (even though there is no NR in the scheme considered in this Appendix), in parallel to the tank's capacitance $C_{\rm T}$. The effect of the qubit on the tank circuit can be described by replacing the tank capacitance $C_{\rm T}$ with $\widetilde{C}_{\rm T} = C_{\rm T} + C_{\rm eff}$, where the effective capacitance of the Cooper-pair box is given by Eq. (B1). The geometric capacitance $C_{\rm geom}$ gives only a constant contribution to the tank capacitance $C_{\rm T}$, while the quantum capacitance $C_{\rm Q} \ll C_0 = C_{\rm T} + C_{\rm geom}$ is defined by the derivative of the average extra Cooper-pair number on the island $\langle n \rangle$.

The tank circuit is biased by the current $I_{\rm b} = I_A \cos\omega_{\rm rf} t$. The output voltage is given by $V_{\rm T} = V_A \cos(\omega_{\rm rf} t + \theta)$. Then from the equation for the voltage we obtain for the phase shift

$$\tan\theta = Q_0 \left(2\frac{\Delta\omega}{\omega_0} + \frac{C_{\rm Q}}{C_0} \right), \qquad \text{(C1)}$$

$$\omega_0 = \frac{1}{\sqrt{L_{\rm T} C_0}}, \; \Delta\omega = \omega_{\rm rf} - \omega_0, \; Q_0 = \frac{1}{R_{\rm T}} \sqrt{\frac{L_{\rm T}}{C_0}}. \qquad \text{(C2)}$$

The measured value can be either the voltage shift θ at resonance frequency ($\Delta\omega = 0$)[12,13,15]

$$\tan\theta = Q_0 \frac{C_{\rm Q}}{C_0}, \qquad \text{(C3)}$$

or the resonance frequency shift (at which the voltage shift $\theta = 0$):[8]

$$\frac{\Delta\omega}{\omega_0} = -\frac{C_{\rm Q}}{2C_0}. \qquad \text{(C4)}$$

Both are proportional to the quantum capacitance $C_{\rm Q}$.

For the sake of illustration, in addition to Fig. 3, we also demonstrate in Fig. 7 the direct LZS interferometry calculated for the quantum capacitance for the parameters of Ref. [14]: $E_{\rm J0}/h = 12.5$ GHz, $E_{\rm C}/h = 24$ GHz, $\omega/2\pi = 4$ GHz, $k_B T/h = 1$ GHz, and also we have taken $\alpha = 0.005$, $B = 0.5$. We note that besides the difference in the parameters, in Fig. 3 the frequency shift $\Delta\omega$ was plotted, while in Fig. 7 the quantum capacitance $C_{\rm Q}$ was shown. Both figures were calculated by numerically solving the Bloch equation.

Finally, it is worthwhile emphasizing that for simplicity we have assumed that the qubit's dynamics is much faster than the

resonator's dynamics. In the general case, the cooperative dynamics of the qubit-resonator system should be studied, as e.g. in Ref. [32]. However, a simplification can be made because the stationary oscillations in the *nonlinear* system (either NR or tank circuit), influenced by the qubit's dynamics, can be reduced to oscillations in the *linear* system, as was studied in Ref. [17]. In that work, the Krylov-Bogolyubov technique of asymptotic expansion was used. This technique describes the influence of the qubit as shifts of both the effective damping factor and the effective coefficient of elasticity. In analogy to the results of Ref. [17], for the system considered here, this means that not only the voltage shift θ is related to the qubit's capacitance $C_{\rm Q}$ [see Eq. (C1)], but also the voltage magnitude V_A is defined by $C_{\rm Q}$. This, in particular, explains the experimental results presented in Fig. 3 by Paila *et al.* [15].

* Electronic address: sshevchenko@ilt.kharkov.ua

[1] M. P. Blencowe, Contemp. Phys. **46**, 249 (2005); M. Poot and H. S. J. van der Zant, http://dx.doi.org/10.1016/j.physrep.2011.12.004.

[2] G. A. Steele, A. K. Hüttel, B. Witkamp, M. Poot, H. B. Meerwaldt, L. P. Kouwenhoven, and H. S. J. van der Zant, Science **325**, 1103 (2009); B. Lassagne, Yu. Tarakanov, J. Kinaret, D. Garcia-Sanchez, and A. Bachtold, *ibid*. **325**, 1107 (2009).

[3] M. A. Sillanpää, J. Sarkar, J. Sulkko, J. Muhonen, and P. J. Hakonen, Appl. Phys. Lett. **95**, 011909 (2009).

[4] J. Q. You and F. Nori, Nature (London) **474**, 589 (2011); Phys. Today **58**(11), 42 (2005).

[5] E. K. Irish and K. C. Schwab, Phys. Rev. B **68**, 155311 (2003).

[6] I. Martin, A. Shnirman, L. Tian, and P. Zoller, Phys. Rev. B **69**, 125339 (2004); M. R. Geller and A. N. Cleland, Phys. Rev. A **71**, 032311 (2005); C. P. Sun, L. F. Wei, Y. X. Liu, and F. Nori, Phys. Rev. A **73**, 022318 (2006); S. Ashhab and F. Nori, Phys. Rev. A **81**, 042311 (2010); Y. X. Liu, A. Miranowicz, Y. B. Gao, J. Bajer, C. P. Sun, and F. Nori, Phys. Rev. A **82**, 032101 (2010).

[7] A. D. O'Connell, M. Hofheinz, M. Ansmann, R. C. Bialczak, M. Lenander, E. Lucero, M. Neeley, D. Sank, H. Wang, M. Weides, J. Wenner, J. M. Martinis, and A. N. Cleland, Nature **464**, 697 (2010).

[8] M. D. LaHaye, J. Suh, P. M. Echternach, K. C. Schwab, and M. L. Roukes, Nature **459**, 960 (2009).

[9] S. N. Shevchenko, S. Ashhab, and F. Nori, Phys. Rep. **492**, 1 (2010).

[10] L. Childress and J. McIntyre, Phys. Rev. A **82**, 033839 (2010); L. Chotorlishvili, Z. Toklikishvili, A. Komnik, and J. Berakdar, Phys. Rev. A **83**, 184405 (2011); S. Miyashita, J. Comp. Theor. Nanoscience **8**, 919 (2011); J. R. Petta, H. Lu, A. C. Gossard, Science **327**, 669 (2010); P. Plötz and S. Wimberger, Eur. Phys. J. D **65**, 199 (2011); H. Ribeiro, J. R. Petta, and G. Burkard, Phys. Rev. B **82**, 115445 (2010); A. Zenesini, D. Ciampini, O. Morsch, and E. Arimondo, Phys. Rev. A **82**, 065601 (2010); J.-N. Zhang, C.-P. Sun, S. Yi, and F. Nori, Phys. Rev. A **83**, 033614 (2011).

[11] N. B. Delone and V. P. Krainov, *Atoms in Strong Light Fields*, Springer Ser. Chem. Phys., Vol. 28, Springer, Berlin–Heidelberg (1985).

[12] M. A. Sillanpää, T. Lehtinen, A. Paila, Yu. Makhlin, L. Roschier, and P. J. Hakonen, Phys. Rev. Lett. **95**, 206806 (2005).

[13] T. Duty, G. Johansson, K. Bladh, D. Gunnarsson, C. Wilson, and P. Delsing, Phys. Rev. Lett. **95**, 206807 (2005); F. Persson, C. M. Wilson, M. Sandberg, and P. Delsing, Phys. Rev. B **82**, 134533 (2010).

[14] M. Sillanpää, T. Lehtinen, A. Paila, Yu. Makhlin, and P. Hakonen, Phys. Rev. Lett. **96**, 187002 (2006).

[15] A. Paila, J. Tuorila, M. Sillanpää, D. Gunnarsson, J. Sarkar, Yu. Makhlin, E. Thuneberg, and P. Hakonen, Quantum Inf. Process. **8**, 245 (2009).

[16] V.I. Shnyrkov, Th. Wagner, D. Born, S.N. Shevchenko, W. Krech, A.N. Omelyanchouk, E. Il'ichev, and H.-G. Meyer, Phys. Rev. B **73**, 024506 (2006); V. I. Shnyrkov, D. Born, A. A. Soroka, and W. Krech, *ibid*. **79**, 184522 (2009).

[17] S.N. Shevchenko, S.H.W. van der Ploeg, M. Grajcar, E. Il'ichev, A.N. Omelyanchouk, and H.-G. Meyer, Phys. Rev. B **78**, 174527 (2008); S.N. Shevchenko, Eur. Phys. J. B **61**, 187 (2008).

[18] D. A. Garanin and R. Schilling, Europhys. Lett. **59**, 7 (2002).

[19] M. V. Berry, J. Phys. A: Math. Theor. **42**, 365303 (2009).

[20] D. Burgarth, K. Maruyama, and F. Nori, Phys. Rev. A **79**, 020305(R) (2009); S. Ashhab, J. R. Johansson, and F. Nori, New J. Phys. **8**, 103 (2006).

[21] Y. Teranishi and H. Nakamura, Phys. Rev. Lett. **81**, 2032 (1998); H. Nakamura, *Nonadiabatic Transition: Concepts, Basic Theories, and Applications*, (World Scientific, Singapore, 2002); B. M. Garraway and N. V. Vitanov, Phys. Rev. A **55**, 4418 (1997).

[22] G. Johansson, L. Tornberg, V.S. Shumeiko and G. Wendin, Condens. Matter **18**, S901 (2006).

[23] E. A. Temchenko, S. N. Shevchenko, and A. N. Omelyanchouk, Phys. Rev. B **83**, 144507 (2011).

[24] W. D. Oliver, Y. Yu, J. C. Lee, K. K. Berggren, L. S. Levitov, and T. P. Orlando, Science **310**, 1653 (2005).

[25] D. A. Garanin and R. Schilling, Phys. Rev. B **66**, 174438 (2002).

[26] G. Sun, X. Wen, B. Mao, J. Chen, Y. Yu, P. Wu, and S. Han, Nat. Commun. **1**, 51 (2010), G. Sun, X. Wen, B. Mao, Y. Yu, J. Chen, W. Xu, L. Kang, P. Wu, and S. Han, Phys. Rev. B **83**, 180507(R) (2011).

[27] P. Huang, J. Zhou, F. Fang, X. Kong, X. Xu, C. Ju, and J. Du, Phys. Rev. X **1**, 011003 (2011).

[28] T. T. Suzuki and Y. Yamauchi, Phys. Rev. A **82**, 042709 (2010).

[29] E. Lucero, M. Hofheinz, M. Ansmann, R. C. Bialczak, N. Katz, M. Neeley, A. D. O'Connell, H. Wang, A. N. Cleland, and J. M. Martinis, Phys. Rev. Lett. **100**, 247001 (2008).

[30] S. Ashhab, J. R. Johansson, A. M. Zagoskin, and F. Nori, Phys. Rev. A **75**, 063414 (2007).

[31] L. Du and Y. Yu, arXiv:1012.2917.

[32] Ya. S. Greenberg and E. Il'ichev, Phys. Rev. B **77**, 094513 (2008).